

Sulfur- and nitrogen-containing porous donor-acceptor polymers as real-time optical and chemical sensors

Yaroslav S. Kochergin,[†] Yu Noda,[†] Ranjit Kulkarni,[†] Klára Škodáková,[‡] Ján Tarábek,[‡] Johannes Schmidt,[†] and Michael J. Bojdys^{†}*

[†]Department of Chemistry, Humboldt-Universität zu Berlin, Brook-Taylor-Str. 2, 12489 Berlin, Germany

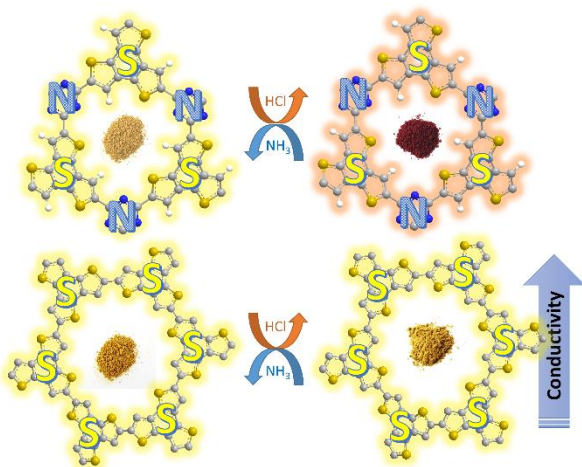
[‡]Institute of Organic Chemistry and Biochemistry of the CAS, Flemingovo nám. 2, 166 10 Prague, Czech Republic

[†]Institute of Chemistry, Technische Universität Berlin, Hardenbergstraße 40, 10623 Berlin, Germany

KEYWORDS

Conjugated microporous polymers, donor-acceptor systems, acid-base sensor, fluorescence sensing, semiconductors.

Table of Contents (TOC)



ABSTRACT

Fully aromatic, organic polymers have the advantage of being composed from light, abundant elements, and are hailed as candidates in electronic and optical devices “beyond silicon”, yet, applications that make use of their π -conjugated backbone and optical bandgap are lacking outside of heterogeneous catalysis. Herein, we use a series of sulfur- and nitrogen-containing porous polymers (SNPs) as real-time optical and electronic sensors reversibly triggered and re-set by acid and ammonia vapors. Our SNPs incorporate donor-acceptor and donor-donor motifs in extended networks and enable us to study the changes in bulk conductivity, optical bandgap, and fluorescence life-times as a function of π -electron de-/localization in the pristine and protonated states. Interestingly, we find that protonated donor-acceptor polymers show a decrease of the optical bandgap by 0.42 eV to 0.76 eV and longer fluorescence life-times. In contrast, protonation of a donor-donor polymer does not affect its bandgap; however, it leads to an increase of electrical conductivity by up to 25-fold and shorter fluorescence life-times. The design strategies highlighted in this study open new avenues towards useful chemical switches and sensors based on modular purely organic materials.

INTRODUCTION

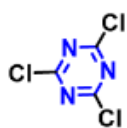
Conjugated microporous polymers (CMPs)¹ attract marked attention as sustainable, noble metal free materials in a wide range of applications such as heterogeneous catalysis,² gas storage and separation,³ energy storage,⁴ optoelectronics,⁵ photovoltaics,⁶ and sensors.⁷ Thanks to their high chemical modularity, exceptional thermal and chemical stability, and a wide array of synthetic approaches, several classes of CMPs have emerged over the last two decades, like polymers of intrinsic microporosity (PIMs),⁸ hyper-cross-linked polymers (HCPs),⁹ covalent organic frameworks (COFs)¹⁰ and their nitrogen-containing analogues - covalent triazine-based frameworks (CTFs).¹¹

Arguably, the most important parameters for the performance of these materials in optoelectronics and catalysis is their bandgap energy and their band structure. These will not only depend on the size and co-planarity of the π -conjugated domains in the polymer backbone, but also on the chemical composition of the building blocks. The most common strategy to vary the bandgap of CMPs relies on changes of the size of the carbon-based, polycyclic building blocks.¹²⁻¹³ Although this bottom-up approach can indeed lead to networks with variable pore sizes and bandgaps, it can also have detrimental effects on the pore structure once pore channels get sufficiently large for inter-penetration of polymer strands to occur. One further strategy to tune the optical bandgap of a conjugated polymer is the incorporation of heteroatom-containing donor-acceptor (D-A) motifs into its backbone.¹⁴⁻¹⁵ Recently, we have introduced a family of sulfur- and nitrogen-containing porous polymers (SNPs) that make use of D-A interactions between neighboring electron-deficient triazine (C_3N_3) cores and electron-rich aryl thiophene building blocks of the polymer to achieve control over the bandgap energy without large changes to the pore structure.¹⁶ In addition, incorporation of aromatic spacers between the donor- and the

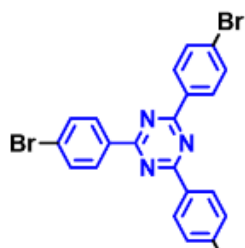
acceptor-domains enabled us to predictively control the strength of donor-acceptor interactions and – by proxy – the extent of charge-carrier recombination in these networks. This has implications for the fluorescence life-times and the outstanding performance in photocatalytic hydrogen evolution from water of these D-A materials.¹⁷⁻¹⁸

In this study, we make use of four key-properties of our conjugated, porous D-A polymers – namely, (1) their strong, covalent backbones, (2) their intrinsic Lewis acidity and basicity, (3) their permanently accessible pore channels to gaseous guest molecules, and (4) their optical bandgaps in the visible part of the spectrum – and we use them as optical and electronic sensors and switches that are triggered by volatile acid vapors and re-set by gaseous ammonia. While colorimetric chemical probes are known from molecular systems in solutions,¹⁹⁻²⁰ or work on the basis of chemical transformations,²¹⁻²³ the here-presented study shows one of the first instances of amorphous porous conjugated polymers used as fully-reversible, colorimetric chemical probes. Recently, we showed, that triazine-containing COFs, made by the same principle, can be also exploited as acid/base chemosensors, thus, highlighting the significance of our approach in view of making multifunctional smart materials.²⁴ Herein, we choose four previously reported SNP systems as reference: **SNP-NDT1**, **SNP-NDT2**, **SNP-BTT1** and **SNP-BTT2** that consist of electron-donating thiophene-based naphthodithiophene (NDT) and benzotrithiophene (BTT) moieties, and electron-withdrawing 1,3,5-triazine (Tz) and tris-phenyltriazine moieties (Scheme 1).¹⁸ In addition, we expand the family of SNPs by three networks, two of which contain a benzodithiophene (BDT) moiety – **SNP-BDT1** and **SNP-BDT2**. To study the effect of D-A dyads *versus* sheer heterocycle content, we further prepare one polymer comprised from electron-rich BTT-building blocks only – **SP-BTT**. All polymers were prepared using the robust, Pd-catalyzed Stille cross-coupling to link the readily available, stannylated derivatives of

thiophene-based molecules with halogenated triazine (TzCl_3) and tris-bromophenyltriazine ($\text{Tz}(\text{PhBr})_3$) or sulfur-containing benzotrithiophene (BTT-Br_3) monomers (see SI and Table S1).^{18, 25}



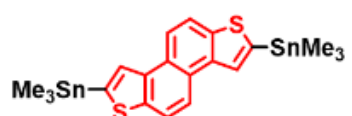
TzCl₃



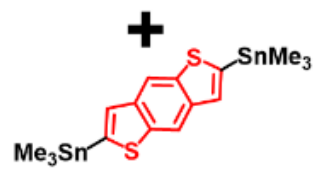
Tz(PhBr)₃



BTT-Br₃



NDT



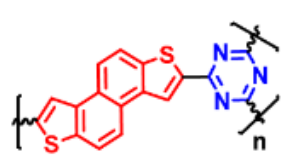
BDT



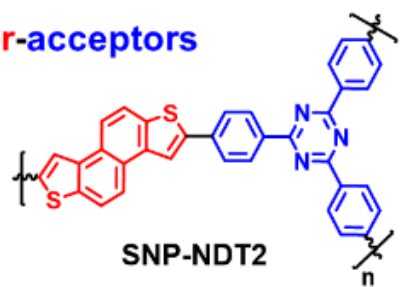
BTT



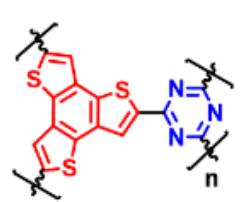
Donor-acceptors



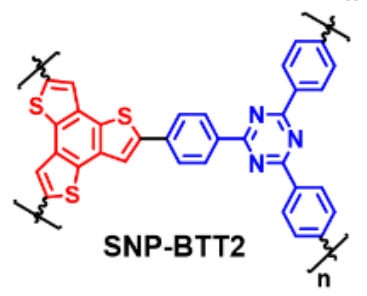
SNP-NDT1



SNP-NDT2

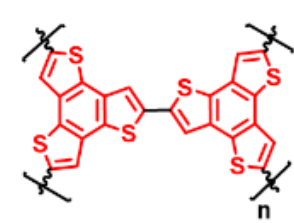


SNP-BTT1



SNP-BTT2

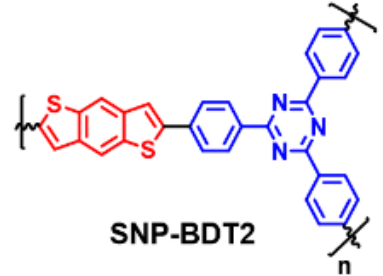
Donor-donor



SP-BTT



SNP-BDT1



SNP-BDT2

Scheme 1. Synthetic pathway towards sulfur- and nitrogen-containing polymers (SNPs) and sulfur-only polymer, **SP-BTT**. Electron-donating thiophene-based linkers (in red) are coupled with electron-accepting triazine-based monomers (in blue) *via* Pd-catalyzed Stille cross-coupling.

EXPERIMENTAL SECTION

Details of all characterization conditions, as well as results of the gas adsorption experiments, PXRD, SEM, TEM, elemental analyses, EDX, XPS, UV-Vis, PL, TCSPC, conductivity, and EPR experiments, which were not included in the main manuscript, are listed in the respective sections of the Supporting Information.

Synthesis of molecular precursors

Syntheses of 2,5,8-tris(trimethylstannyl)benzo[1,2-b:3,4-b':5,6-b''] (**BTT**), 2,7-bis(trimethylstannyl)naphtho[2,1-b:6,5-b']dithiophene (**NDT**), 2,6-bis-trimethylstannanyl-benzo[1,2-b;4,5-b']dithiophene (**BDT**), 2,4,6-tris(4-bromophenyl)-1,3,5-triazine (**Tz(PhBr)₃**) and 2,5,8-tribromobenzo[1,2-b:3,4-b':5,6-b'']trithiophene (**BTT-Br₃**) are given in the Supporting Information (Scheme S1-S4).

General procedure for Stille-coupling polymerisation

An overview of all prepared materials can be found in Table S1.

The respective stannylated monomer, brominated monomer, and Pd(PPh₃)₄ (3:2:5% mol ratio; in case of benzo[1,2-b:3,4-b':5,6-b'']trithiophene (**BTT**) – 1:1:5% mol ratio) were dissolved in anhydrous toluene under inert atmosphere and refluxed for 3 days. In a short time period (1-2 h) the precipitate of polymer started to appear in the reaction flask. After completion of the reaction the precipitate was filtered and washed with hot toluene, DMF, chloroform, THF and methanol (3 times each solvent). Subsequently, Soxhlet extraction was performed using chloroform, THF,

and methanol (24 h each solvent). Afterwards the solid was dried in a vacuum drying oven at 120 °C for 24 h. More detailed reaction parameters can be found in Table S2.

RESULTS AND DISCUSSION

Structure and chemical composition of the polymer systems were confirmed *via* ^{13}C cross-polarization magic-angle-spinning (CP-MAS) NMR spectroscopy, combustion elemental analysis (EA), X-ray photoelectron spectroscopy (XPS), and thermogravimetric analysis (TGA). Both the triazine- and thiophene-containing **SNP-BDT1** and **SNP-BDT2** polymers have characteristic signals at 167-169 ppm in solid-state ^{13}C CP-MAS spectra which belong to C_3N_3 -ring carbons. Signals in the range from 110-150 ppm are attributed to sp^2 -hybridised carbon atoms within aromatic phenyl and thiophene units (Figure S2). The sulfur-containing polymer, **SP-BTT**, shows three distinct signals at 136, 131 and 118 ppm, which correspond to quaternary carbons in thiophene and phenyl rings, and to tertiary thiophene carbons. Details of the bulk analysis of the as-received polymers are found in the SI (Table S2, S4-S7, Figure S12-S17). For all polymer systems, we detect residual Pd-content (0.03 to 1.05 wt%) and P atoms (0.09 to 0.36 wt%) trapped in the polymer matrix after the cross-coupling reaction, as well as Sn (0.39 to 1.07 wt%) and halogen atoms (Cl: 0.57 to 3.72 wt%, Br: 2.25 to 5.74 wt%) arising from unreacted end-groups. These findings correlate with results from TGA measurements under an oxidative atmosphere that show a residual content of non-combustible inorganics between 3 and 7 wt% (Figure S4a). Irrespective, the high degree of cross-linking we achieve in all networks confers high thermal stability up to 750 °C under an inert atmosphere (Figure S4b).

Powder X-ray diffraction (PXRD) shows that the **SNP-BDT1**, **SNP-BDT2** and **SP-BTT** networks are – just like the previously reported SNPs – amorphous with broad features at around 10 and 25° 2 θ which correlate with in-plane distances between aromatic building blocks and π -

stacking distances of approx. 3.6 Å,¹¹ respectively (Figure S5).¹⁶⁻¹⁸ Scanning electron microscopy (SEM) images of **SNP-BDT1** and **SNP-BDT2** networks confirm a ‘cauliflower’-like morphology typical for nucleation-growth polymers, while the **SP-BTT** polymer grows in rod-like aggregates of 20 to 100 μm length (Figure S6-S8). Transmission electron microscopy (TEM) and selected-area electron-diffraction (SAED) for these three polymers confirm a similar degree of internal, microscopic structure as seen in PXRD data with visible, concentric rings indicative of polycrystalline materials (Figure S9-S11). Cross-linking of C_2 and C_3 symmetric building blocks suggests a regular bonding pattern with hexagonal, “honeycomb”-shaped pores on paper, and the low number of unreacted end-groups in our polymers suggests just that. However, as structural analysis reveals and as we established previously,²⁶ Pd-catalyzed Stille cross-coupling favors the formation of the disordered, kinetic product, presumably with some degree of interpenetration of adjacent pore structures. We investigated these pore channels by nitrogen gas adsorption/desorption analysis performed at 77 K. All polymers show Type I isotherms with a pronounced hysteresis indicative of micro- and mesopores (Figure S3).²⁷ The guest accessible surface area was calculated according to Brunauer–Emmett–Teller (BET) and varies in the range from 79 to 698 m² g⁻¹ (Table 1).

So far, we have established the covalent bonding pattern of our networks and their permanent micro- and mesoporosity. Further, we make use of their intrinsic π -aromaticity and heteroatom content by exposing these polymers to a trigger: corrosive HCl vapors. In principle, SNPs have two Lewis-basic sites that can be protonated – triazine-ring nitrogens and thiophene sulfur atoms. **SP-BTT** plays a particular role in this study, since it contains thiophene-moieties only (Scheme S5). The as-received powders of SNPs show a rapid color change and marked red-shift of the absorption edge in solid-state UV-Vis spectra (Figure 1a, S18-22, Video S1). These values

correspond to a decrease of the direct optical bandgap by 0.45 to 0.66 eV and indirect optical bandgap by 0.42 to 0.76 eV according to the Kubelka-Munk function (Figure 1c, S18-S22).²⁸ The most sensitive network, **SNP-NDT1**, is triggered by hydrochloric acid concentrations as low as 54 ppm (dosing limit of the current setup, see SI); a response that can still be distinguished by the naked eye within 30 seconds (Figure S25, Table S9). In contrast, sulfur-containing **SP-BTT** does not show any appreciable color change when exposed to HCl vapors, hence, no marked changes in UV-Vis absorption (Figure 1b) and in optical bandgaps (Figure 1d), respectively. One conceivable explanation for this phenomenon could be the difference in basicity between the triazine and the thiophene moiety. While 1,3,5-substituted triazines are readily protonated at the pyridinic ring-nitrogen,²⁹ thiophenes and oligothiophenes are protonated by superacids only at the 2-position.³⁰⁻³¹

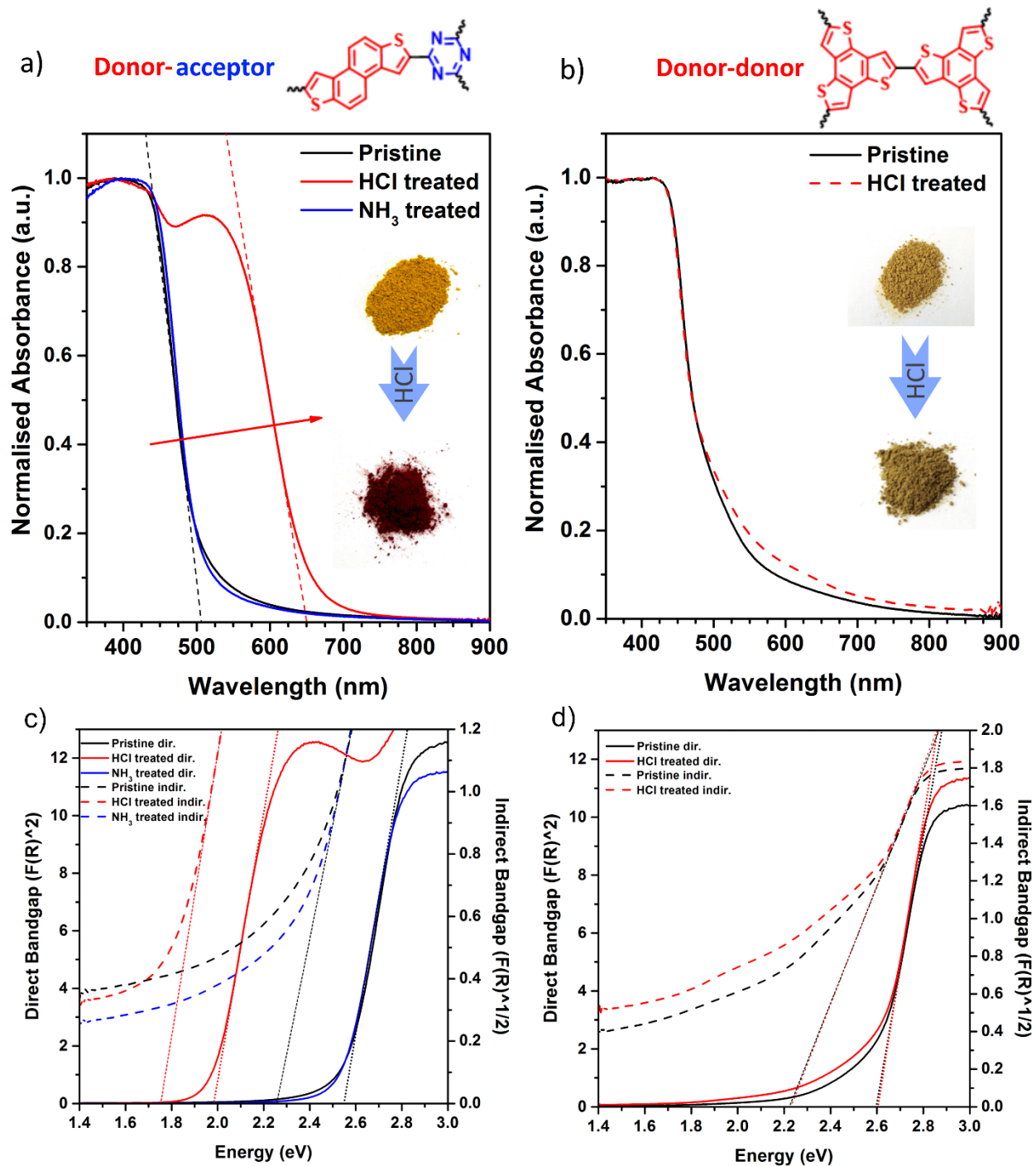


Figure 1. a) Repeating unit of SNP-NDT1 and solid-state UV-Vis absorption spectra and c) Tauc plot of SNP-NDT1 in pristine state (black), after exposure to HCl (red) and NH₃ (blue) vapors. In the inset of (a) – photographs of polymer before and after protonation; c) Repeating unit of SP-

BTT and solid-state UV-Vis absorption spectra and d) Tauc plot of **SP-BTT** in pristine state (black) and after exposure to HCl (red) vapor. In the inset of (c) – photographs of polymer before and after protonation.

Notably, this coloration can be fully re-set when the HCl-treated polymer is exposed to NH₃ vapors from 24% aqueous ammonia solution (Figure 1a, c, S1). This on/off response to HCl/NH₃ vapors can be triggered at least five consecutive times (as shown for **SNP-NDT1**, Figure S26) with no apparent losses in the intensity of the optical response.

We closely examined the chemical composition of the polymer backbone during this on/off response to verify that the interaction of the polymer with corrosive HCl is indeed a reversible chemisorption process. Fourier-transform infrared (FT-IR) spectra of pristine and HCl-treated samples show characteristic C₃N₃-ring vibrations around 1500 cm⁻¹ and 1360-1370 cm⁻¹, along with the triazine-ring breathing mode at 805-820 cm⁻¹ (Figure S28-33).³²⁻³³ Moreover, there are no indicative signals in the OH- and NH- region around 3000 cm⁻¹ that would be a tell-tale sign of irreversible hydrolysis of the polymers. Similarly, FT-IR spectra of the pristine and HCl treated **SP-BTT** polymer show C-S vibrations of the thiophene ring at 810 cm⁻¹ as well as aromatic C-C stretching at 1342 cm⁻¹ (Figure S34).²⁶ A comparison of FT-IR spectra over five cycles of exposure to HCl/NH₃ gases shows that all reported networks remain chemically stable (Figure S35). Previous DFT calculations confirm that the Lewis basic N-atoms of the triazine moieties are the preferred site of protonation.²⁴

This rapid and fully-reversible detection of HCl vapors at low concentrations makes SNPs suitable candidates for naked-eye sensors. Moreover, we monitored the response of **SNP-NDT1** to different acids, such as hydrobromic, nitric, sulfuric, trifluoromethylsulfonic (TFMSA), and

acetic acid. Initial exposure for 1 min revealed color changes only in case of HCl. Longer exposure for up to 3 days ensured complete diffusion of acid vapors throughout the material. Accordingly, we also observed marked color change in case of HBr and HNO₃, whereas vapors of TFMSA and acetic acid caused only slight shifts of the UV-Vis absorption edge (Figure S27). Interestingly, sulfuric acid shifted the absorption edge of **SNP-NDT1** towards the blue region by ~12 nm; an electron induction effect into the polymer network which probably stems from a strong interaction of the SO₄²⁻ anion with the polymer network, analogous to charge-transfer complexes formed between sulfate and molecular electron acceptors.³⁴⁻³⁵ Overall, we observe that soft conjugate bases (e.g. AcO⁻) cause a smaller UV-Vis shift than hard conjugate bases (e.g. Cl⁻). This phenomenon merits further study, but a conceivable explanation is that more localised charge-transfer complexes with hard conjugate bases are responsible for a larger UV-Vis shift than weaker, more delocalised CT complexes with soft conjugate bases, as observed previously.³⁶

Previously we discovered, that SNPs are highly fluorescent in benzene suspensions under UV-light irradiation.¹⁸ Here we confirmed the fluorescence of obtained materials in solid state, including newly synthesized frameworks (Figure S36). Absolute quantum yields (AQY) measured under 365 nm UV light irradiation vary from 0.3% (at 79.5% absorbance) for **SNP-NDT1** to 1.0% (at 79.9% absorbance) for **SNP-NDT2** (Table S10). We performed solid-state photoluminescence emission (PLE) measurements in steady-state and time-correlated single photon counting (TCSPC) experiments to better understand, how the protonation event influences the optical properties of the materials. As expected, PLE spectra recorded at 440 nm excitation wavelength revealed marked red-shift of the emission maximum after protonation,

with emission maxima appearing in the near IR region up to 788 nm for **SNP-BDT1** (Figure S37).

Table 1. Porous, optical and electronic properties of SNPs.

| Network | S_{BET} (m² g⁻¹)^[a] | E_{g.dir.} (eV)^[b] | E_{g.indir.} (eV)^[c] | PL_{max} (nm)^[d] | τ_{avg} (ns)^[e] | ρ (μS m⁻¹)^[f] |
|---------------------|---|--|--|--|---|--|
| SNP-NDT1* | 656 | 2.56 | 2.27 | 559 | 0.58 | 0.048 |
| SNP-NDT1-HCl | - | 1.98 | 1.75 | 717 | 1.11 | 0.051 |
| SNP-NDT2* | 79 | 2.50 | 2.33 | 547 | 1.06 | 0.055 |
| SNP-NDT2-HCl | - | 1.85 | 1.58 | 753 | 1.85 | 0.055 |
| SNP-BTT1* | 698 | 2.57 | 2.26 | 545 | 0.54 | 0.055 |
| SNP-BTT1-HCl | - | 2.09 | 1.83 | 718 | 1.89 | 0.017 |
| SNP-BTT2* | 411 | 2.60 | 2.38 | 525 | 0.37 | 0.049 |
| SNP-BTT2-HCl | - | 2.08 | 1.84 | 740 | 1.33 | 0.066 |
| SNP-BDT1 | 195 | 2.38 | 2.00 | 632 | 0.41 | 0.353 |
| SNP-BDT1-HCl | - | 1.75 | 1.53 | 788 | 1.03 | 0.258 |
| SNP-BDT2 | 92 | 2.36 | 2.19 | 553 | 0.57 | 0.061 |
| SNP-BDT2-HCl | - | 1.82 | 1.51 | 773 | 1.03 | 0.057 |
| SP-BTT | 356 | 2.60 | 2.23 | 532 | 0.37 | 0.415 |
| SP-BTT-HCl | - | 2.60 | 2.23 | 532 | 0.49 | 10.371 |

[a] Surface area calculated from N₂ adsorption isotherm using BET equation; [b] Direct and [c] indirect optical bandgaps calculated *via* the Kubelka-Munk function; [d] Maximum of photoluminescence emission measured in solid state; [e] Average fluorescence lifetimes (τ) were calculated from triple-exponential fitting of fluorescence decay; [f] Conductivity values (ρ) were obtained from I-V profile measurements with bias sweep of -10 to 10 V, triplicates of each sample were conducted and an average was taken.*- the S_{BET}, E_{g dir} and E_{g indir} data for SNP-NDT1, SNP-NDT2, SNP-BTT1 and SNP-BTT2 polymers was taken from previous report by us.¹⁸

These findings are in a good agreement with UV-Vis study – the observed decrease of the optical bandgap width corresponds to a lower transition energy to the excited state, hence, to longer

emission wavelengths in fluorescence decay. Average fluorescence life-times estimated by triple-exponential fitting from TCSPC for the pristine polymers are in the range from 0.37 ns for **SNP-BTT2** and **SP-BTT** to 1.06 ns for **SNP-NDT2** (Figure 2a, Table 1, S10). After exposure to HCl, however, we observe a 2- to 3-fold increase in fluorescence life-times for triazine-containing polymers from 1.03 ns for **SNP-BDT1-HCl** and **SNP-BDT2-HCl** up to 1.89 ns for **SNP-BTT1-HCl** (Figure 2b, Table 1, S10). The results indicate, that after protonation charge carriers are in general more localized, which will lead to fewer non-radiative charge recombination events, and hence, longer fluorescence lifetimes. Here, we can appreciate the advantage of the modular make-up of SNPs: strong donor-acceptor interactions in SNPs that contain directly linked triazine- and thiophen-moieties enable more efficient charge transfer – and, hence, comparatively faster exciton decay – than their counterparts where D and A moieties are separated by an aryl spacer.³⁷⁻³⁹

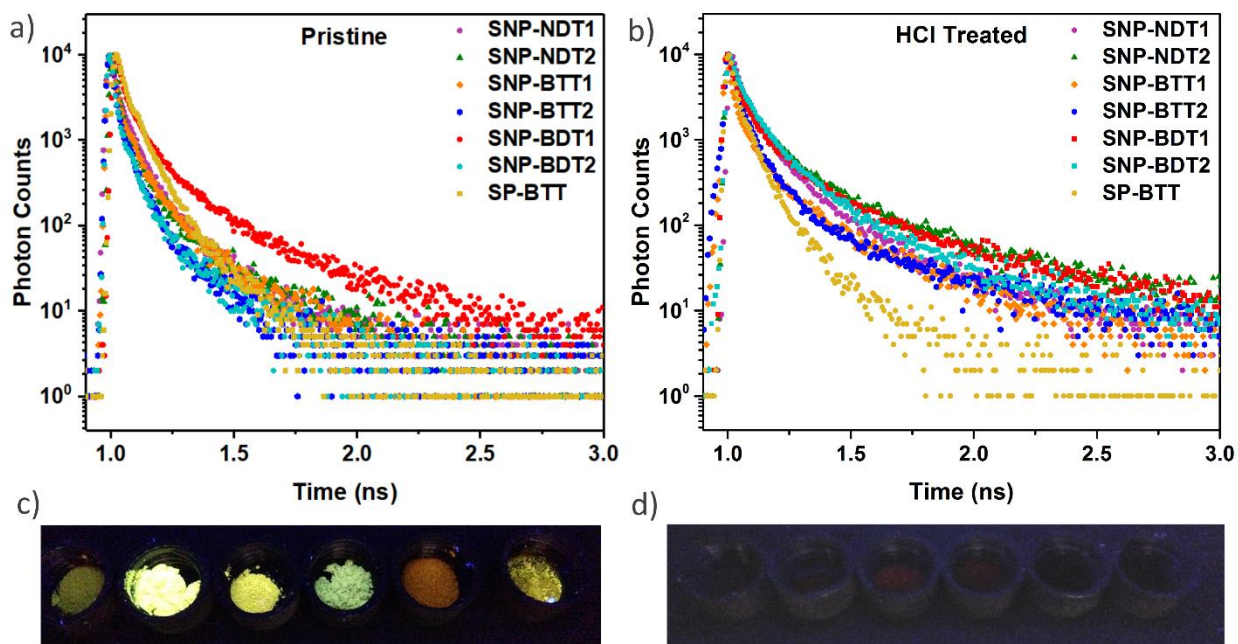


Figure 2. Time-correlated fluorescence decay for pristine (a) and HCl treated (b) polymers; photographs of fluorescence in solid state of pristine (c) and protonated (d) SNPs (from left to right: **SNP-NDT1**, **SNP-NDT2**, **SNP-BTT1**, **SNP-BTT2**, **SNP-BDT1**, and **SNP-BDT2**; $\lambda_{exc} = 365$ nm).

Notably, the sulfur-containing **SP-BTT** network did not show such dramatic increases in fluorescence life-times with a total change from 0.37 to 0.49 ns in the HCl-treated network. In this case, charge carriers are more delocalized due to the absence of strong D-A interactions. This small increase in fluorescence life-times in **SP-BTT** can be explained by a partial transfer of electron density from the central benzene ring of the benzotrithiophene core. It is worth to note, that the fluorescence intensity of SNPs in the solid state is completely quenched to the naked eye after exposure to HCl vapors after 30 seconds, and it is fully recovered after exposure to ammonia (Figure 2c, d). This feature can be used for manufacturing of acid-base fluorescence sensors.

Protonation of the heteroatoms has an influence on the bandgap width and photoluminescence, and it involves charge transport across the π -aromatic network as a whole. Such an increase of charge carrier mobility was reported for *p*-type doping of semiconducting, linear polymers.⁴⁰⁻⁴² Thus, we examined the influence of protonation on the charge carrier mobility of our bulk materials using two-probe measurements (Figure S38-S46). Interestingly, there is only a slight measurable increase of conductivity within the same order of magnitude for all SNPs upon activation with HCl vapors (Table 1, Figure S45). However, the thiophene-only **SP-BTT** framework showed a dramatic increase in conductivity after protonation from 0.415 to 10.371 $\mu\text{S m}^{-1}$ (Figure 3a). These results support the fact that donor-acceptor interactions within polymer network will tailor not only optical, but also electronic properties of the desired

materials. As seen in the UV-Vis study, protonated triazine-containing SNPs have more localized charges – presumably in the form of Cl-salts stabilized by strong D-A interactions – that do not contribute much to overall bulk conductivity, whereas **SP-BTT** experiences a higher degree of charge-delocalization and thus showing higher charge carrier mobility.

In the end, we monitored the change in paramagnetic behavior of prepared polymers upon protonation using electron paramagnetic resonance (EPR) spectroscopy (Figure 3b, S47). All pristine materials show the presence of paramagnetic species typical for polymeric networks with extended π -conjugation.⁴³⁻⁴⁵ The EPR signals are centered around g -values ranging from 2.0035 to 2.0045 (linewidth of about 0.47 to 1.26 mT, Table S11) indicating the contribution of heteroatoms to overall charge localization. After exposure to HCl vapors all SNPs show a decrease in EPR signal intensity with the exception of **SNP-NDT1** – a polymer that is made up of directly coupled, strongly interacting D-A domains. This supports the hypothesis that charge localization is enhanced by stronger donor-acceptor interactions (Figure S47). Again, the homo-coupled, sulfur-containing **SP-BTT** network is the outlier: there is a marked increase in EPR signal intensity after protonation (Figure 3b). Quantitative analysis of the EPR spectra of **SP-BTT** shows a 2-times increase of radical concentration from $(7\pm 0.2)\cdot 10^{13}$ radicals mg^{-1} (0.12 ± 0.02 nmol mg^{-1}) to $(1.4\pm 0.2)\cdot 10^{14}$ radicals mg^{-1} (0.23 ± 0.03 nmol mg^{-1}) in the protonated state. In the light of the I-V conductivity results, this suggests that protonation leads to an increased delocalization of paramagnetic species and that these paramagnetic species could be contributing to the conductivity of HCl-treated **SP-BTT**.

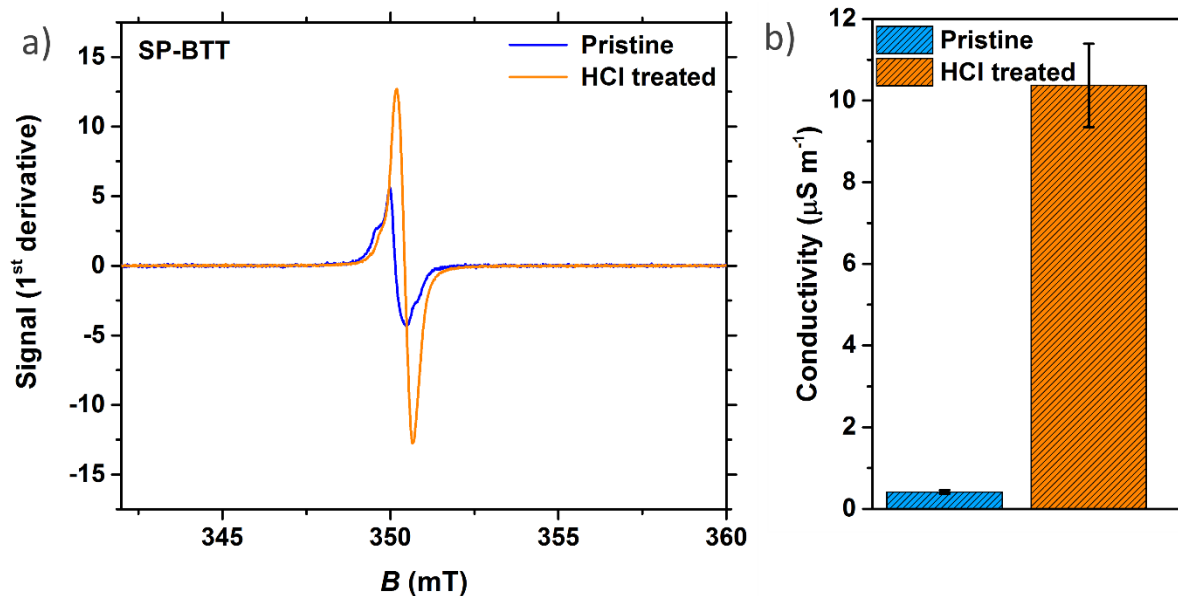


Figure 3. a) EPR spectra and b) direct conductivity measurements of **SP-BTT** in the pristine (blue) and the protonated (orange) state.

To compare charge transfer properties of **SP-BTT** we performed temperature dependent EPR measurements taking **SNP-NDT1** – the most strongly interacting D-A polymer – as a reference. Computational simulations were based on the assumption that one to two protons are present per D-A dyad after HCl exposure (Figure S48 and Table S12), and they correlate well with the observed EPR spectra. The *g*-factor exhibits a hysteresis upon heating and cooling (Figure S49). These observations indicate that the variations of the *g*-factor are not related to the increased structural mobility of the heated network, but rather to the delocalization of unpaired electrons.⁴⁶ The *g*-factor of both polymers increases upon heating, and it increases further upon cooling for **SNP-NDT1**. Here, both polymers are switched to a “more localized” spin state. However, **SP-BTT** is better at delocalizing radical paramagnetic centers along the polymeric chain in comparison to **SNP-NDT1** (Figure S50).

CONCLUSION

In summary, we present a comprehensive study that correlates optical and electronic effects in weakly and strongly interacting donor-acceptor systems based on the family of highly modular, sulfur and nitrogen-containing porous polymers (SNPs). SNPs are capable of real-time, reversible optical and electronic sensing of volatile acid and base vapors. The optical and electronic responses involve the entirety of the π -conjugated polymer, and the host-guest interactions between volatile trigger molecules and the chemoresponsive polymer are made possible by the permanent porosity, strong, covalent backbone and predictably modular heteroatom content of the materials. The optical on-response of strongly D-A interacting networks is selective for acid vapors with small counter anions (such as HCl, HBr and HNO₃) that are able to form more localized chromophore complexes. Conversely, the weakly interacting, thiophene-only D-D polymer benefits from overall charge delocalization and a 25-fold enhancement of charge carrier mobility when exposed to acid vapors. These findings demonstrate that D-A polymers are suitable materials for chemically triggered optical sensors and switches, while homo-coupled D-D polymers are useful electronic chemosensors and switches.

Supporting Information.

The Supporting Information is available free of charge on the ACS Publications website at DOI: xxxxx

Corresponding Author

*E-mail: m.j.bojdys.02@cantab.net

Author Contributions

Y.S.K. conceived and designed experiments, performed synthetic experiments, analyzed the data, and wrote the paper. Y.N. performed direct conductivity measurements and analyzed the data. R.K. performed BET measurements. K.Š. performed synthetic experiments, FTIR measurements, and analyzed the data. J.T. performed EPR measurements and analyzed the data. J.S. performed XPS and analyzed the data. M.J.B. contributed reagents/materials/analysis tools. M.J.B. conceived and designed experiments, analyzed the data, and wrote the paper. All authors have given approval to the final version of the manuscript.

Notes

The authors declare no competing financial interests.

ACKNOWLEDGMENT

We thank André Sanches for help with monomers synthesis and upscaling as well as assistance with UV-Vis measurements, Ranjit Kulkarni and Pavla Eliášová for N₂ sorption measurements, Stanislava Matějková for ICP-OES, Lucie Bednarova for IR spectroscopy measurements, Martin Dračinský for access to solid-state NMR facilities, and Dr. Miroslav Štěpánek for solid-state fluorescence measurements. J.S. acknowledges support from the German Science Foundation (Project TH1463/15-1) and the Cluster of Excellence (UniCat). M.J.B. thanks the European Research Council (ERC) for funding under the Starting Grant Scheme (BEGMAT-678462).

REFERENCES

1. Cooper, A. I., Conjugated microporous polymers. *Advanced Materials* **2009**, *21* (12), 1291-1295.
2. Kessler, F. K.; Zheng, Y.; Schwarz, D.; Merschjann, C.; Schnick, W.; Wang, X.; Bojdys, M. J., Functional carbon nitride materials — design strategies for electrochemical devices. *Nat. Rev. Mater.* **2017**, *2*, 17030.
3. Chang, Z.; Zhang, D.-S.; Chen, Q.; Bu, X.-H., Microporous organic polymers for gas storage and separation applications. *Phys. Chem. Chem. Phys.* **2013**, *15* (15), 5430-5442.
4. Yan, K.; Yanhong, X.; Zhaoqi, G.; Donglin, J., Supercapacitive Energy Storage and Electric Power Supply Using an Aza-Fused π -Conjugated Microporous Framework. *Angew. Chem. Int. Ed.* **2011**, *50* (37), 8753-8757.
5. Ostroverkhova, O., Organic Optoelectronic Materials: Mechanisms and Applications. *Chemical Reviews* **2016**, *116* (22), 13279-13412.
6. Shun, W.; Jia, G.; Jangbae, K.; Hyotcherl, I.; Donglin, J., A Belt-Shaped, Blue Luminescent, and Semiconducting Covalent Organic Framework. *Angew. Chem. Int. Ed.* **2008**, *47* (46), 8826-8830.

7. Yang, J. S.; Swager, T. M., Fluorescent porous polymer films as TNT chemosensors: Electronic and structural effects. *Journal of the American Chemical Society* **1998**, *120* (46), 11864-11873.
8. Budd, P. M.; Ghanem, B. S.; Makhseed, S.; McKeown, N. B.; Msayib, K. J.; Tattershall, C. E., Polymers of intrinsic microporosity (PIMs): robust, solution-processable, organic nanoporous materials. *Chem. Commun.* **2004**, (2), 230-231.
9. Shujun, X.; Yali, L.; Bien, T., Recent Development of Hypercrosslinked Microporous Organic Polymers. *Macromol. Rapid Commun.* **2013**, *34* (6), 471-484.
10. Côté, A. P.; Benin, A. I.; Ockwig, N. W.; O'Keeffe, M.; Matzger, A. J.; Yaghi, O. M., Porous, Crystalline, Covalent Organic Frameworks. *Science* **2005**, *310* (5751), 1166-1170.
11. Kuhn, P.; Antonietti, M.; Thomas, A., *Angew. Chem. Int. Ed.* **2008**, *47* (18), 3450-3453.
12. Sprick, R. S.; Jiang, J.-X.; Bonillo, B.; Ren, S.; Ratvijitvech, T.; Guiglion, P.; Zwiijnenburg, M. A.; Adams, D. J.; Cooper, A. I., *J. Am. Chem. Soc.* **2015**, *137* (9), 3265-3270.
13. Meier, C. B.; Sprick, R. S.; Monti, A.; Guiglion, P.; Lee, J.-S. M.; Zwiijnenburg, M. A.; Cooper, A. I., Structure-property relationships for covalent triazine-based frameworks: The effect of spacer length on photocatalytic hydrogen evolution from water. *Polymer* **2017**, *126*, 283-290.
14. Li, L.; Lo, W.-y.; Cai, Z.; Zhang, N.; Yu, L., Donor–Acceptor Porous Conjugated Polymers for Photocatalytic Hydrogen Production: The Importance of Acceptor Comonomer. *Macromolecules* **2016**, *49* (18), 6903-6909.
15. Kailasam, K.; Mesch, M. B.; Möhlmann, L.; Baar, M.; Blechert, S.; Schwarze, M.; Schröder, M.; Schomäcker, R.; Senker, J.; Thomas, A., Donor–Acceptor-Type Heptazine-Based Polymer Networks for Photocatalytic Hydrogen Evolution. *Energy Technology* **2016**, *4* (6), 744-750.
16. Schwarz, D.; Kochergin, Y. S.; Acharjya, A.; Ichangi, A.; Opanasenko, M. V.; Čejka, J.; Lappan, U.; Arki, P.; He, J.; Schmidt, J.; Nachtigall, P.; Thomas, A.; Tarábek, J.; Bojdys, M. J., *Chem. - Eur. J.* **2017**, *23* (53), 13023-13027.
17. Schwarz, D.; Acharjya, A.; Ichangi, A.; Lyu, P.; Opanasenko Maksym, V.; Gößler Fabian, R.; König Tobias, A. F.; Čejka, J.; Nachtigall, P.; Thomas, A.; Bojdys Michael, J., Fluorescent Sulphur- and Nitrogen-Containing Porous Polymers with Tuneable Donor–Acceptor Domains for Light-Driven Hydrogen Evolution. *Chem. - Eur. J.* **2018**.
18. Kochergin, Y. S.; Schwarz, D.; Acharjya, A.; Ichangi, A.; Kulkarni, R.; Eliášová, P.; Vacek, J.; Schmidt, J.; Thomas, A.; Bojdys, M. J., Exploring the “Goldilocks Zone” of Semiconducting Polymer Photocatalysts by Donor–Acceptor Interactions. *Angewandte Chemie International Edition* **2018**, *57* (43), 14188-14192.
19. Oweyung, R. E.; Panzer, M. J.; Sonkusale, S. R., Colorimetric Gas Sensing Washable Threads for Smart Textiles. *Scientific Reports* **2019**, *9* (1), 5607.
20. Belger, C.; Weis, J. G.; Egap, E.; Swager, T. M., Colorimetric Stimuli-Responsive Hydrogel Polymers for the Detection of Nerve Agent Surrogates. *Macromolecules* **2015**, *48* (21), 7990-7994.
21. Yoon, J.; Chae, S. K.; Kim, J.-M., Colorimetric Sensors for Volatile Organic Compounds (VOCs) Based on Conjugated Polymer-Embedded Electrospun Fibers. *J. Am. Chem. Soc.* **2007**, *129* (11), 3038-3039.
22. Yin, M.; Ji, C., Nanoscaled Fluorescent Films and Layers for Detection of Environmental Pollutants. In *Nanoscaled Films and Layers*, IntechOpen, Laszlo Nanai 2014.

23. Feng, L.; Musto, C. J.; Kemling, J. W.; Lim, S. H.; Zhong, W.; Suslick, K. S., Colorimetric Sensor Array for Determination and Identification of Toxic Industrial Chemicals. *Anal. Chem* **2010**, *82* (22), 9433-9440.
24. Kulkarni, R.; Noda, Y.; Kumar Barange, D.; Kochergin, Y. S.; Lyu, P.; Balcarova, B.; Nachtigall, P.; Bojdys, M. J., Real-time optical and electronic sensing with a β -amino enone linked, triazine-containing 2D covalent organic framework. *Nature Communications* **2019**, *10* (1), 3228.
25. Stille, J. K., The Palladium-Catalyzed Cross-Coupling Reactions of Organotin Reagents with Organic Electrophiles [New Synthetic Methods (58)]. *Angew. Chem. Int. Ed.* **1986**, *25* (6), 508-524.
26. Kim, M.-S.; Phang, C. S.; Jeong, Y. K.; Park, J. K., *Polym. Chem.* **2017**, *8* (37), 5655-5659.
27. Sing, K. S. W.; Everett, D. H.; Haul, R. A. W.; L. Moscou; Pierotti, R. A.; Rouquerol, J.; Siemieniewska, T., *Pure Appl. Chem.* **1985**, *57*, 603-619.
28. Kubelka, P.; Munk, F., *Z. Tech. Phys.* **1931**, 593-601.
29. Meier, H.; Holst, Hans C.; Oehlhof, A., Star-Shaped Compounds Having 1,3,5-Triazine Cores. *European Journal of Organic Chemistry* **2003**, *2003* (21), 4173-4180.
30. Yu, Y.; Gunic, E.; Miller, L. L., Protonation of Oligothiophenes. *Chemistry of Materials* **1995**, *7* (2), 255-256.
31. Feng, Q.; Luo, S.; Olmstead, M.; Rauchfuss, T. B.; Stafford, P. R., Activation of Thiophenes by Superacids: Protonation and Polymerization. *Chemistry of Materials* **1997**, *9* (3), 641-643.
32. Kuecken, S.; Acharjya, A.; Zhi, L.; Schwarze, M.; Schomacker, R.; Thomas, A., *Chem. Commun.* **2017**, *53* (43), 5854-5857.
33. Schwarz, D.; Noda, Y.; Klouda, J.; Schwarzová-Pecková, K.; Tarábek, J.; Rybáček, J.; Janoušek, J.; Simon, F.; Opanasenko, M. V.; Čejka, J.; Acharjya, A.; Schmidt, J.; Selve, S.; Reiter-Scherer, V.; Severin, N.; Rabe, J. P.; Ecorchard, P.; He, J.; Polozij, M.; Nachtigall, P.; Bojdys, M. J., Twinned Growth of Metal-Free, Triazine-Based Photocatalyst Films as Mixed-Dimensional (2D/3D) van der Waals Heterostructures. *Adv. Mater.* **2017**, *29* (40), 1703399.
34. Samanta, S.; Dey, P.; Ramesh, A.; Das, G., A solo fluorogenic probe for the real-time sensing of SO₃²⁻ and SO₄²⁻/HSO₄⁻ in aqueous medium and live cells by distinct turn-on emission signals. *Chemical Communications* **2016**, *52* (68), 10381-10384.
35. Bąk, K. M.; Masłowska, K.; Chmielewski, M. J., Selective turn-on fluorescence sensing of sulfate in aqueous-organic mixtures by an uncharged bis(diamidocarbazole) receptor. *Organic & Biomolecular Chemistry* **2017**, *15* (28), 5968-5975.
36. Panda, P.; Veldman, D.; Sweelssen, J.; Bastiaansen, J. J. A. M.; Langeveld-Voss, B. M. W.; Meskers, S. C. J., Charge Transfer Absorption for π -Conjugated Polymers and Oligomers Mixed with Electron Acceptors. *The Journal of Physical Chemistry B* **2007**, *111* (19), 5076-5081.
37. Xu, Y.; Nagai, A.; Jiang, D., Core-shell conjugated microporous polymers: a new strategy for exploring color-tunable and -controllable light emissions. *Chem. Commun.* **2013**, *49* (16), 1591-1593.
38. Dai, P.; Yang, L.; Liang, M.; Dong, H.; Wang, P.; Zhang, C.; Sun, Z.; Xue, S., Influence of the Terminal Electron Donor in D-D- π -A Organic Dye-Sensitized Solar Cells: Dithieno[3,2-b:2',3'-d]pyrrole versus Bis(amine). *ACS Appl. Mater. Interfaces* **2015**, *7* (40), 22436-22447.
39. Jiang, J.-X.; Trewin, A.; Adams, D. J.; Cooper, A. I., *Chem. Sci.* **2011**, *2* (9), 1777-1781.

40. Zalar, P.; Kuik, M.; Henson, Z. B.; Woellner, C.; Zhang, Y.; Sharenko, A.; Bazan, G. C.; Nguyen, T.-Q., Increased Mobility Induced by Addition of a Lewis Acid to a Lewis Basic Conjugated Polymer. *Adv. Mater.* **2013**, *26* (5), 724-727.
41. Blinova, N. V.; Stejskal, J.; Trchová, M.; Prokeš, J., Control of polyaniline conductivity and contact angles by partial protonation. *Polym. Int.* **2007**, *57* (1), 66-69.
42. McManus, P. M.; Cushman, R. J.; Yang, S. C., *J. Phys. Chem.* **1987**, *91* (3), 744-747.
43. Katsoulidis, A. P.; Dyar, S. M.; Carmieli, R.; Malliakas, C. D.; Wasielewski, M. R.; Kanatzidis, M. G., Copolymerization of terephthalaldehyde with pyrrole, indole and carbazole gives microporous POFs functionalized with unpaired electrons. *J. Mater. Chem. A*, **2013**, *1* (35), 10465-10473.
44. Fischer, S.; Schmidt, J.; Strauch, P.; Thomas, A., An Anionic Microporous Polymer Network Prepared by the Polymerization of Weakly Coordinating Anions. *Angew. Chem. Int. Ed.* **2013**, *52* (46), 12174-12178.
45. Bildirir, H.; Paraknowitsch, J. P.; Thomas, A., A Tetrathiafulvalene (TTF)-Conjugated Microporous Polymer Network. *Chem. Eur. J.* **2014**, *20* (31), 9543-9548.
46. Bajžíková, K.; Kohout, M.; Tarábek, J.; Svoboda, J.; Novotná, V.; Vejpravová, J.; Pocięcha, D.; Gorecka, E., All-organic liquid crystalline radicals with a spin unit in the outer position of a bent-core system. *J. Mater. Chem. C* **2016**, *4* (48), 11540-11547.